RSC Advances

ROYAL SOCIETY OF CHEMISTRY

www.rsc.org/advances

RSC Advances

ARTICLE

Synthesis and properties of the derivatives of triphenylamine and 1,8-naphthalimide with the olefinic linkages between chromophores

Received 00th January 20xx,
Accepted 00th January 20xx

DOI: 10.1039/x0xx00000x

www.rsc.org/

Dalius Gudeika,[a] Gjergji Sini,[b] Vygintas Jankauskas,[c] Galyna Sych,[a] and Juozas V. Grazulevicius[a,*]

Two donor-acceptor type molecules consisting of triphenylamine and 1,8-naphthalimide moieties with the olefinic linkages between chromophores were synthesized by Heck reaction. The compounds obtained are capable to form molecular glasses with glass transition temperatures of 56 and 75 °C recorded for mono- and di-substituted derivatives of triphenylamine, respectively. They exhibit high thermal stabilities with 5% weight loss temperatures of 350 and 363 °C. Fluorescence quantum yields of the dilute solutions of the synthesized compounds range from 0.065 to 0.72 while those of the solid films are 0.028 and 0.034. The Stokes shifts increased with the increase of the solvent polarity. Cyclic voltammetry measurements revealed close values of the solid state ionization potentials (5.22 and 5.27 eV) and of electron affinities (-3.20 and -3.18 eV). For the layer of the monosubstituted derivative of triphenylamine core hole mobility was found to be 2.1×10^{-3} $cm^2V^{-1}s^{-1}$. Good intrinsic hole transport parameters were theoretically estimated in the frame of Marcus theory, and the impact of polaron-type hole transport in these materials is discussed.

Keywords: donor-acceptor, olefinic linkage, triphenylamine, 1,8-naphthalimide, charge-transport.

INTRODUCTION

Compounds having an intramolecular charge transfer (ICT) properties usually consist of electron donating (D) and electron accepting (A) groups linked through a π-conjugated bridge which makes it possible to reduce the band gap between ionization potential and electron affinity values. Donor-π-acceptor (D-π-A) type organic compounds are regarded as promising organic semiconducting materials due to their broad absorption in the visible region resulted from ICT, easy tuned electronic energy levels and band gaps through adjusting the acceptor, donor, and π-conjugated bridge moieties.[1,2]

So far, among the different classes of organic π-conjugated systems reported, the derivatives of electron donating triphenylamine (TPA) have been widely investigated as hole transporting materials for organic light emitting diodes (OLEDs) and other optoelectronic devices.[3-7] Owing to the noncoplanarity of the phenyl rings, TPA derivatives can be viewed as 3D systems and their combination with linear π-conjugated systems can be expected to lead to amorphous molecular materials with good hole-transporting capability.[8-12] It is well known that the central nitrogen atom is responsible for the donor behavior of arylamine compounds which are widely investigated and used in various optoelectronic and electronic devices, such as dye-sensitized solar cells,[13] OLEDs,[14] organic field-effect transistors,[15] non-linear optical devices,[16] and sensors.[17] Numerous experimental and theoretical studies were carried out in order to find correlations between the structure and properties of the derivatives of TPA.[18-22]

So far, the use of the concept of A-D system in 1,8-naphthalimide chemistry was rather limited. Much attention has been paid to the design and synthesis of new 1,8-naphthalimide architectures. The optical, photophysical, photoelectrical, electrochemical properties of 1,8-naphthalimide derivatives are determined by the nature of the substituents. Linking of electron donating groups at C-4 position of the naphthalic ring gives a "push-pull" electronic configuration and generate ICT excited states.[23-25] This ICT character leads to a large excited-state dipole moment and broad absorption and emission bands at longer wavelengths. ICT transition is highly solvent dependent, and the photophysical properties of the compounds with ICT character, such as the wavelengths of the maxima of absorption and emission spectra, the fluorescence lifetimes as well as the fluorescence quantum yields, are all affected by the properties of solvents.[26]

Recently, we reported on the synthesis of the electroactive compounds containing electron donating TPA fragments as cores and electron accepting 1,8-naphthalimide moieties as

[a] Department of Polymer Chemistry and Technology, Kaunas University of Technology, Radvilenu pl. 19, LT-50254 Kaunas, Lithuania.
[b] Laboratoire de Physicochimie des Polymères et des Interfaces, EA 2528 Université de Cergy-Pontoise, 5 mail Gay-Lussac, 95031 Cergy-Pontoise.
[c] Department of Solid State Electronics, Vilnius University, Sauletekio aleja 9, LT-10222 Vilnius, Lithuania.
* Corresponding author: Juozas V. Grazulevicius; Fax: +37037 300152; Tel: +37037 300193; E-mail: juozas.grazulevicius@ktu.lt.
Electronic SupplementaryInformation (ESI) available: ^{1}H NMR and ^{13}C NMR spectra of compounds, theoretical absorption spectra of model compounds, selected choice of dimers constructed from the model compound. See DOI: 10.1039/x0xx00000x

arms.[27-29] Introduction of ethenyl or ethynyl units as spacers helped the compounds to acquire planarity.

In this work, two new charge transporting derivatives TPA and 1,8-naphthalimide with the olefinic linkages between electrophores were designed and synthesized with the aim of getting the further information of the structure-properties relationship of the donor-acceptor derivatives.

EXPERIMENTAL METHODS

Instrumentation

Melting points (Mp) of the compounds were estimated using Electrothermal Mel-Temp apparatus. ^{1}H NMR and ^{13}C NMR spectra were obtained on Varrian Unity Inova (300 MHz for ^{1}H), 75.4 MHz for ^{13}C). Mass (MS) spectra were recorded with Waters ZQ 2000. Elemental analysis was carried out with an Exeter Analytical CE-440 Elemental Analyzer. Infrared (IR) spectra were recorded using Perkin Elmer Spectrum GX spectrometer. Differential scanning calorimetry (DSC) measurements were carried out using a Perkin-Elmer DSC-7 series thermal analyzer at a heating rate of 10 ^{o}C/min under nitrogen flow. Thermogravimetric analysis (TGA) was performed on a Mettler Toledo TGA/SDTA 851^e. UV spectra were recorded with Hitachi U-3000 spectrometer. Fluorescence measurements of the dilute solutions and of the solid films of the compounds were performed using spectrometer FS980. For these measurements, the dilute solutions of the investigated compounds were prepared by dissolving them in a spectral grade solvent at 10^{-5} M concentration. The drop-casting from THF solutions (10^{-3} M) was employed to prepare thin solid films of the compounds. Fluorescence quantum yields (Φ_F) of the solutions were estimated by using integrated sphere method.[30] Cyclic voltammetry (CV) measurements were carried out by a three-electrode assembly cell from Bio-Logic SAS and a micro-AUTOLAB Type III potentiostat-galvanostat. The measurements were carried out in a solution of dry dichloromethane containing 0.5 M tetrabutylammonium hexafluorophosphate (Bu_4NPF_6) at 25 ^{o}C, scan rate 50 mV/s, sample concentration 10^{-5} M. The potentials were measured against $Ag/AgNO_3$ as reference electrode, platinum wire was used as counter electrode. The experiments were calibrated with the standard ferrocene/ferrocenium (Fc/Fc^+) redox system.[31]

The ionization potentials (IP_{PE}) of the layers of the compounds were measured by the electron photoemission method in air.[32] The samples were fabricated by means of vacuum deposition of the compounds onto Al coated glass substrate under vacuum below $5\cdot10^{-6}$ mbar. The negative voltage of 500 V was supplied to the sample substrate. Then the layers were illuminated with the monochromatic light from the deep UV deuterium light source ASBN-D130-CM and CM110 1/8m monochromator. The counter-electrode was connected to the input of the 6517B Keithley electrometer for the photocurrent measurement. The photocurrent was strongly dependent on the incident light photon energy. An energy scan of the incident photons was performed while increasing the photon energy. In this scan direction, no electrons were emitted until the photon energy exceeded the ionization potential (IP_{PE}) of the compounds.

Hole mobilities (μ_h) of the layers of the compounds and of their molecular mixtures with bisphenol Z polycarbonate (PC-Z) were estimated by xerographic time-of-flight (XTOF) method as described earlier.[33] The electric field was created by positive corona charging. The charge carriers were generated at the layer surface by illumination with pulses of nitrogen laser (pulse duration was 1 ns, wavelength 337 nm). As a result of pulsed illumination the layer surface potential decreased down to 1-5% of the initial potential. The capacitance probe connected to the wide frequency band electrometer measured the rate of the surface potential decrease dU/dt. The transit time t_t for the samples with the transporting material was determined from the kink of the curve of the dU/dt transient in log-log scale. The hole-drift mobility was calculated by using the formula $\mu=d^2/U_0t_t$, where d is the layer thickness, and U_0 the surface potential at the moment of illumination. The layers were casted from the solutions of compounds **4**, **5** in THF. The substrates were glass plates with a conductive polyester films with an Al layer. After coating and drying at the room temperature the samples were heated at 80 ^{o}C for 1 h. The thickness of the charge-transporting layers varied in the range of 2.8-6.0 μm.

Materials

4-Bromo-1,8-naphthalic anhydride, 2-ethylhexylamine were purchased from TCI, triphenylamine, triethylamine (TEA), palladium acetate(II) ($Pd(OAc)_2$), tri-*tert*-butylphosphine solution, 1.0 M in toluene (tri(*o*-tolyl)$_3$), acrolein diethyl acetal, tetrabutylammonium acetate (*n*-Bu_4NOAc), *N*-bromosuccinimide (NBS) were purchased from Aldrich and used as received. Dimethylformamide (DMF, Lachema) was dried by distillation over CaH_2. THF was dried and distilled over sodium and benzophenone. Dichloromethane (POCH), ethyl acetate and *n*-hexane (Penta) were purified and dried using the standard procedures.[34]

4-Bromo-*N*-(2-ethylhexyl)-1,8-naphthalimide (**BrIM**),[35] m.p. 82-83 ^{o}C, *N,N*-diphenyl-4-bromoaniline (**1a**),[36] m.p. 106-107 ^{o}C, bis(4-bromophenyl)phenylamine (**1b**),[37] (E)-4-(4-(diphenylamino)phenyl)acrylaldehyde, (**2a**),[38] m.p. 97-98 ^{o}C, *N*-(4-((E)-buta-1,3-dienyl)phenyl)-*N*-phenylbenzenamine (**2b**),[39] (E)-4-{4-[(E)-4-formyl-1-ethenyl]-(4,4'-(diphenylamino)phenyl)}acrylaldehyde (**3a**),[40] m.p. 121-122 ^{o}C were prepared according to the published procedures.

***N,N*-Bis(4-((E)-buta-1,3-dienyl)phenyl)benzenamine (3b).** A mixture of (E)-4-{4-[(E)-4-formyl-1-ethenyl]-(4,4'-(diphenylamino)phenyl)}acrylaldehyde (**3a**) (0.5 g, 1.42 mmol), sodium *tert*-butoxide (0.34 g, 3.55 mmol) and methyltriphenylphosphonium bromide (1.21 g, 3.41 mmol) in dry THF under nitrogen was heated with stirring at 80 ^{o}C for 24 h. After cooling to the room temperature, the mixture was poured into distilled water and extracted with chloroform. The organic layer was dried with anhydrous magnesium sulfate and concentrated by vacuum evaporation. The crude product was purified by column chromatography (*n*-hexane/ethyl acetate

vol. ratio 9:1) to obtain amorphous compound **3b** with the yield of 0.24 g (52%). R_f=0.32 (*n*-hexane/ethyl acetate 9:1); ^{1}H NMR (300 MHz, $CDCl_3$, 25 ^{o}C, δ, ppm): 7.32-7.25 (m, 6H, -Ar), 7.14-7.11 (m, 2H, 2×-CH=CH-CH=CH_2), 7.09-7.05 (m, 3H, -Ar, 2×-CH=CH-CH=CH_2), 6.79-6.66 (m, 8H, -Ar, 2×-CH=CH-CH=CH_2), 5.32 (d, 2H, *J* = 10.1 Hz, -CH=CH-CH=CH_2), 5.16 (d, 2H, *J* = 10.1 Hz, -CH=CH-CH=CH_2). ^{13}C NMR (75.4 MHz, $CDCl_3$, 25 ^{o}C, δ, ppm): δ=141.4, 141.2, 134.7, 130.8, 128.9, 127.4, 126.4, 124.5, 123.3, 122.7, 118.4, 115.6. MS (APCI$^+$, 20 V): m/z: 350 ($[M+H]^+$). IR, (KBr), cm^{-1}: 3025 ν (CH_{ar}); 2958, 2878 ν ($CH_{aliphatic}$); 1655, 1581, 1498 ν (C=C_{ar}); 1358, 1325, 1266 ν (C-N); 967 γ (*trans*, -CH=CH-CH=CH_2); 772, 754, 688 γ (CH_{ar}). Elemental analysis calc (%) for $C_{26}H_{23}N$: C 89.36, H 6.63, N 4.01; found C 89.33, H 6.67, N 4.04.

***N*-(4-((E)-Buta-1,3-dienyl)phenyl)-*N*-phenyl-(*N*-(2-ethylhexyl)-1,8-naphthalimide) (4)**. A flask was charged with a mixture of **BrIM** (0.50 g, 1.29 mmol), **3a** (0.46 g, 1.55 mmol), $Pd(OAc)_2$ (3.6 mg, 0.016 mmol), P(*o*-tolyl)$_3$ (16 mg, 0.071 mmol), DMF (10 mL) and triethylamine (3 mL). The flask was degassed and purged with nitrogen. The mixture was heated at 90 ^{o}C for 24 h under nitrogen. Then, it was filtered and the filtrate was poured into methanol. The orange precipitate was filtered off and washed with methanol. The crude product was purified by silica gel column chromatography using the mixture of ethyl acetate and hexane (1:8, V:V) as an eluent to obtain **4** as red crystals with the yield of 0.42 g (54%). It was recrystallized from the mixture of solvents of the eluent. R_f=0.41 (*n*-hexane/ethyl acetate 8:1); M.p. = 182 – 183 ^{o}C. ^{1}H NMR spectrum (300 MHz, $CDCl_3$, 25 ^{o}C, δ, ppm): 8.64 (dd, 1H, J_1 = 7.2 Hz, J_2 =2.8 Hz, -Ar), 8.57 (dd, 1H, J_1 = 4.8 Hz, J_2 =2.8 Hz, -Ar), 8.55 (d, 1H, *J* = 4.8 Hz, -Ar), 7.97 (d, 1H, *J* = 7.2 Hz, -Ar), 7.78 (dd, 1H, J_1 = 8.5 Hz, J_2 = 7.2 Hz, -Ar), 7.47-7.33 (m, 6H, -Ar), 7.29-7.23 (m, 2H, -CH=CH-CH=CH-), 7.19-7.12 (m, 4H, -Ar, -CH=CH-CH=CH-), 7.10-6.99 (m, 5H, -Ar), 6.82 (d, 1H, *J* = 8.5 Hz, -Ar), 4.33-4.03 (m, 2H, -CH_{aliph}), 2.04-1.93 (m, 1H, -CH_{aliph}), 1.49-1.26 (m, 8H, -CH_{aliph}), 1.02-0.86 (m, 6H, -CH_{aliph}). ^{13}C NMR (75.4 MHz, $CDCl_3$, 25 ^{o}C, δ, ppm): 164.8, 148.6, 147.3, 141.3, 137.8, 134.2, 133.5, 131.8, 129.3, 129.3, 129.2, 129.1, 128.9, 128.0, 127.2, 126.4, 125.8, 125.8, 125.8, 123.5, 123.2, 123.1, 122.7, 122.6, 122.5, 121.3, 44.6, 37.2, 31.8, 29.1, 25.3, 23.6, 14.4, 11.9. IR, (KBr), cm^{-1}: 3032 ν (CH_{ar}); 2956, 2928, 2858 ν ($CH_{aliphatic}$); 1697 ν (C=O_{imide}); 1660, 1583, 1505, 1488 ν (C=C_{ar}); 1354, 1332, 1274 ν (C-N); 988 γ (*trans*, -CH=CH-CH=CH); 778, 754, 693 γ (CH_{ar}). MS (APCI$^+$, 20 V): m/z: 605 ($[M+H]^+$). Elemental analysis calc (%) for $C_{42}H_{40}N_2O_2$: C 83.41, H 6.67, N 4.63, O 5.29; found C 83.44, H 6.65, N 4.59.

***N,N*-Bis(4-((E)-buta-1,3-dienyl)phenyl)phenyl bis(*N*-(2-ethylhexyl)-1,8-naphthalimide) (5)** was prepared by the similar procedure as **4** using **3b** (0.5 g, 1.42 mmol), **BrIM** (1.22 g, 3.14 mmol), $Pd(OAc)_2$ (8.02 mg, 0.036 mmol), P(*o*-tolyl)$_3$ (32 mg, 0.14 mmol). The crude product was purified by silica gel column chromatography using the mixture of ethyl acetate and hexane (1:8, V:V) as an eluent to obtain **5** as red crystals with the yield of 0.51 g (37%). It was recrystallized from the mixture of solvents of the eluent. R_f=0.39 (*n*-hexane/ethyl acetate 8:1); M.p. = 155 – 156 ^{o}C. ^{1}H NMR (300 MHz, $CDCl_3$, 25 ^{o}C, δ, ppm): 8.62 (dd, 2H, J_1 = 7.7 Hz, J_2 =4.9 Hz, -Ar), 8.55 (dd, 3H, J_1 = 9.8 Hz, J_2 =4.9 Hz, -Ar), 7.96 (dd, 2H, J_1 = 7.7 Hz, J_2 =4.9 Hz, -Ar), 7.80-7.75 (m, 3H, -Ar), 7.48-7.39 (m, 6H, -Ar), 7.35-7.28 (m, 4H, -Ar, 2×-CH=CH-CH-CH=CH-), 7.26-7.15 (m, 5H, -Ar, 2×-CH=CH-CH=CH-), 7.13-6.99 (m, 4H, -Ar), 6.62 (d, 2H, *J* = 9.8 Hz, -Ar), 4.19-4.08 (m, 4H, -CH_{aliph}), 2.01-1.91 (m, 2H, -CH_{aliph}), 1.44-1.30 (m, 16H, -CH_{aliph}), 1.00-0.85 (m, 12H, -CH_{aliph}). ^{13}C NMR (75.4 MHz, $CDCl_3$, 25 ^{o}C, δ, ppm):165.3, 148.2, 143.9, 141.2, 140.5, 137.8, 137.3, 133.2, 131.9, 129.3, 129.3, 128.2, 128.2, 127.8, 127.5, 126.2, 125.9, 125.6, 125.3, 125.2, 123.2, 123.2, 122.7, 122.4, 122.3, 44.3, 37.2, 31.9, 29.3, 25.3, 23.4, 14.3, 11.3. IR, (KBr), cm^{-1}: 3048 ν (CH_{ar}); 2953, 2926, 2862 ν ($CH_{aliphatic}$); 1699 ν (C=O_{imide}); 1659, 1582, 1501, 1479 ν (C=C_{ar}); 1353, 1330, 1278 ν (C-N); 981 γ (*trans*, -CH=CH-CH=CH); 779, 751, 697 γ (CH_{ar}). MS (APCI$^+$, 20 V): m/z: 965 ($[M+H]^+$). Elemental analysis calc (%) for $C_{66}H_{65}N_3O_4$: C 82.21, H 6.79, N 4.36, O 6.64; found C 82.25, H 6.72, N 4.33.

Computational details

The calculations in this study were carried out in the frame of density functional methods (DFT).[41] B3LYP[42,43] functional was used for the calculation of molecular properties, whereas the ωB97X-D[44] functional was used during the geometry optimizations of dimers constituted from like molecules. The geometry of all molecules in their neutral and cationic states were optimized without symmetry constraints by using the 6-31G(d,p) basis set. The vertical ionization potentials (I_p) were calculated at the neutral state geometry as energy difference between neutral and cation species. All calculations were performed by using the Gaussian 09 program.[45]

The absorption spectra of compounds **4** and **5** were obtained by means of time dependent DFT (TDDFT)[46-50] calculations at the B3LYP/6-31G(d,p) level. The theoretical absorption bands were obtained by using Gausview (version 5) software.[51]

The internal reorganization energies (λ_i) for holes were calculated by mean of the following equation:[52]

$$\lambda_i = (E_M^{M^+} - E_M^M) + (E_{M^+}^M - E_{M^+}^{M^+}) \quad (1)$$

with E_M^{+M}, for instance, being the energy of the cationic species (M^+) in the geometry of the neutral molecule (*M*).

For each model dimer, the HOMO-HOMO electronic couplings were calculated at the B3LYP/ 6-31G(d,p) level, by using the fragment orbital method (also known as the "direct calculation" or "two state model").[53-55]

RESULTS AND DISCUSSION

Synthesis and characterization

Scheme 1 shows the synthetic routes to the target compounds. The first step was condensation of 4-bromo-1,8-naphthalic anhydride (**BrA**) with 2-ethylhexylamine in DMF which gave 4-bromo-*N*-(2-ethylhexyl)-1,8-naphthalimide (**BrIM**). Compounds **1a,b** were prepared by bromination of **TPA** with NBS. The reactions of **1a,b** with acrolein diethyl acetal afforded cinnamaldehydes **2a,b**. Compounds **3a,b** were

prepared by the reactions of cinnamaldehydes **2a,b** with methyltriphenylphosphonium bromide. The final steps were Heck reactions of **BrIM** with **3a,b** in the presence of palladium(II) acetate and tri-o-tolylphosphine to obtain the target compounds **4** and **5**. All the derivatives were characterized by ^{1}H and ^{13}C NMR, mass spectrometries and elemental analysis. The target compounds (**4, 5**) were found to be soluble in various organic solvents such as dichloromethane (DCM), chloroform, tetrahydrofuran (THF), toluene and *etc.*

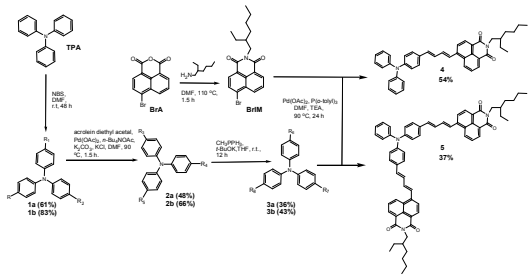

	R	R_1	R_2		R_3	R_4	R_5		R_6	R_7	R_8
1a	H	Br	H	2a	H		H	3a	H		H
1b	Br	Br	H	2b			H	3b			H

Scheme 1. The synthetic routes to **4, 5**.

Thermal properties

The thermal properties of compounds **4, 5** were investigated by thermogravimetric analysis (TGA) and differential scanning calorimetry (DSC) under a nitrogen atmosphere. The values of glass transition temperatures (T_g), melting points (T_m) and 5% weight loss temperatures ($T_{ID-5\%}$) are summarized in Table 1.

Table 1. Thermal characteristics of compounds **4** and **5**.

Compound	T_g [°C][a] (2^{nd} heating)	T_m [°C][b]	$T_{ID-5\%}$ [°C][c]
4	56	191	350
5	75	159	363

[a] T_g is glass transition temperature, [b] T_m is melting point, (both estimated by DSC), [c] $T_{ID-5\%}$ is 5% weight loss temperature estimated by TGA at a heating rate of 10 °C/min in N_2 atmosphere.

Compounds **4** and **5** were isolated after the synthesis as crystalline compounds, however they could be transformed into the glassy state by heating from the melts. Their behavior in DSC experiments was similar, therefore DSC curves of only one compound (**4**) are given in Figure 1a. $T_{ID-5\%}$ for **4** and **5** were observed at 350 and 363 °C, respectively (Figure 1b). These values indicate the relatively high thermal stability of the compounds. $T_{ID-5\%}$ increased with increase of the number of naphthalimide arms. These results are in agreement the previously reported data on the thermal stability of the other derivatives of naphthalimide and TPA.[27,28]

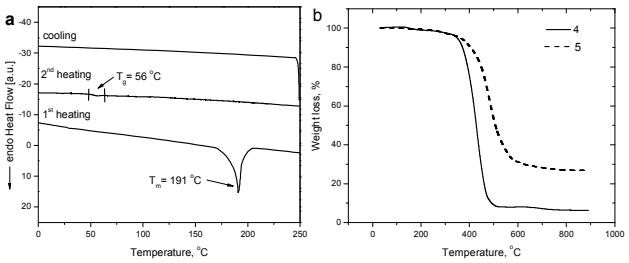

Figure 1. (a) DSC thermograms of **4**; (b) TGA curves of **4** and **5**.

In the first heating scans compounds **4** and **5** revealed endothermic melting peaks at 191 and 159 °C, respectively. No crystallization was observed during the cooling scans. In the second heating scans compounds **4** and **5** showed glass transitions at 56 and 75 °C, respectively and no crystallization was observed on the following heating. T_g values of **4** and **5** were slightly lower than those of the earlier reported corresponding derivatives of naphthalimide and TPA with the different (shorter) linkages between the chromophores.[27-29]

Geometry and electronic properties of model compounds

The geometrical structures of the model compounds **M4** and **M5** are shown in Figure 2. While the three N-C bonds are situated in the same plane ("N-plane"), a propeller-like geometry is found around the TPA N atoms. Ph-"N-plane" dihedral angles are larger for the non-substituted *versus* substituted phenyl groups (-44.5° and -34.3°, respectively in the case of compound **M4**, and -46.5° and -37.7° in the case of **M5**). The effect of TPA-butadiene linking appears through shortening of N-C(Ph) distances and decreasing of Ph-"N-plane" dihedral angles. However, there is less free room for two short N-C distances in the case of **M5** as compared to **M4**, which is consequently reflected in larger Ph-"N-plane" dihedral angles for **M5**. The butadiene moieties lie in the same plane as the internal TPA phenyl groups, but form dihedral angles of roughly 25° with the naphthalimide group(s).

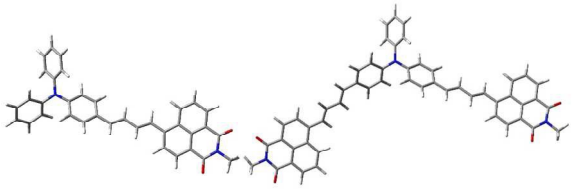

Figure 2. Geometrical structures of model compounds **M4** and **M5**, containing methyl groups instead of ethyl-hexyl ones (B3LYP/6-31G(d,p) level in "gas phase").

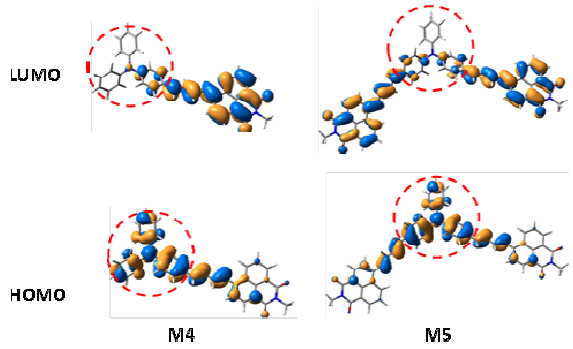

Figure 3. HOMO and LUMO representations of compounds **M4** and **M5**. The red dashed circles delimit the TPA moiety.

HOMO and LUMO of model compounds **M4** and **M5** are given in Figure 3. Both HOMOs are basically localized on the TPA and butadiene moieties (Figure 3), with the dominant contribution coming from the TPA moiety. Similarly, the naphthalimide and butadiene moieties are found to contribute to the LUMOs, with practically no contribution from the TPA core.

The energies of the frontier orbitals are given in Table 2. Both HOMO and LUMO energies decrease with increasing number of naphthalimide-butadiene- groups. This is the expected result for LUMO energies, due to some degree of interaction between the two branches. The decrease in HOMO energy seems to depend on two effects: while the attractor effect of naphthalimide groups may contribute to this effect, the increasing Ph-"N-plane" dihedral angles in the order **M4** < **M5** also plays in the same sense. However, the evolution of LUMO energy is faster than for HOMO, so that the HOMO-LUMO gap is by 0.08 eV smaller for **M5** than for **M4**.

Electrochemical and photoelectron emission properties

The electrochemical properties of compounds **4** and **5** were investigated by CV. As it is shown in Figure 4 compounds **4** and **5** showed ambipolar redox behavior with only one quasi-reversible oxidation and reduction couple waves around -1.5 and 1.5 V respectively (*vs.* $Ag/AgNO_3$). The results of the electrochemical measurements are listed in Table 2. The reduction peak is predetermined by withdrawing nature of naphthalimide moieties, while one quasi-reversible oxidation peak is predetermined by the electron donating nature of TPA moiety.[14] Compound **5** possesses the slightly lower onset oxidation potential than compound **4**. In the reductive potential region, the reduction processes started at -1.60 and -1.63 V, for compounds **4** and **5,** respectively. As a result, electrochemical band gaps of compounds **4** and **5** were found to be comparable (2.05 and 2.04 eV, respectively). These values are somewhat lower than the corresponding optical band gap (E_g^{opt}) values observed for the solutions of **4, 5** (Table 2). Similar E_g^{opt} and E_g^{elc} values were also observed for the previously reported TPA and naphthalimide derivatives.[26,27] The solid state ionization potentials (IP_{CV}) of **4** and **5** were found to be very close, 5.25 and 5.22 eV, respectively. A similar observation applies to electron affinities (EA_{CV}) of -3.20 and -3.18 eV, respectively. These values are comparable to those of the other derivatives of TPA and naphthalimide.[27,28]

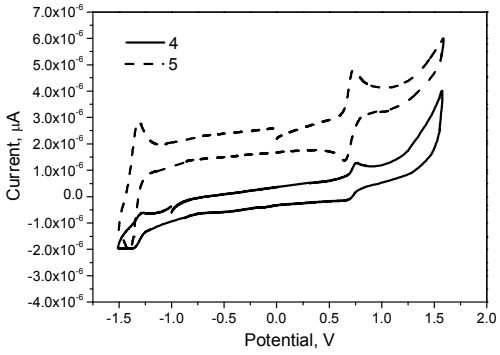

Figure 4. CV curves of **4** and **5** (10^{-5} M solutions in CH_2Cl_2 with 0.1 M *n*-Bu_4NPF_6).

Table 2. Electrochemical characteristics of **4** and **5**.

Compound	E_{onset}^{ox} *vs* $Fc/V^{(a)}$	E_{onset}^{red} *vs* $Fc/V^{(a)}$	IP_{CV}, (eV)[(b)]	EA_{CV}, (eV)[(b)]	E_g^{elc}, (eV)[(c)]	E_g^{opt} (eV)[(d)]	IP_{PE} (IP^V) (eV)[(e)]	ε_{HOMO} (eV)[(f)]	ε_{LUMO} (eV)[(f)]	E_{H-L} (eV)[(g)]
4	0.45	-1.60	5.25	-3.20	2.05	2.12	5.47 (6.09)	-5.02	-2.49	2.53
5	0.42	-1.63	5.22	-3.18	2.04	2.09	5.49 (5.98)	-5.09	-2.64	2.45

[a] E_{onset}^{ox} and E_{onset}^{red} measured *vs* Fc/Fc^+; [b] Ionization potentials and electron affinities estimated according to $IP_{CV} = (E_{onset}^{ox} + 4.8)$ [eV]. $EA_{CV} = -(E_{onset}^{red} + 4.8)$ [eV] (where, E_{onset}^{ox} and E_{onset}^{red} are the onset reduction and oxidation potentials *versus* the Fc/Fc^+). E_{onset}^{ox} and E_{onset}^{red} of Fc/Fc^+ measured in DCM solution containing 0.1 M Bu_4NPF_6 was 0.275 V *vs* Fc/Fc+); [c] $E_g^{elc} = |IP_{CV}| - |EA_{CV}|$, where E_g^{elc} is the electrochemical band gap; [d] The optical band gap estimated from the onset wavelength of optical absorption of dilute solution, according to the formula: $E_g^{opt} = E/e$, where $e = 1.6\times10^{-19}$ C, $E = hc/\lambda_{edge}$, $h = 6.63\times10^{-34}$ Js, and $c = 3.0\times10^{8}$ m/s, in which the λ_{edge} is the onset value of absorption spectra in long wave direction; [e] IP_{PE} corresponds to the electron photoemission IP values. IP^V are the theoretical vertical IP (given in parentheses); [f] HOMO (ε_{HOMO}) and LUMO (ε_{LUMO}) energies, and [g] HOMO-LUMO gap (E_{H-L}) for model compounds **M4** and **M5** (B3LYP/6-31G(d,p), gas phase).

The solid state ionization potentials (IP_{PE}) of the synthesized compounds were also estimated by the electron photoemission technique under ambient conditions. Figure 5 shows the electron photoemission spectra of the films of compounds **4** and **5**. Comparable values of IP_{PE} of 5.47 and 5.49 eV were established for compounds **4** and **5** by extrapolation of the linear parts of the spectra to zero photocurrent. The ionization potentials established by electron photoemission spectrometry were slightly higher than those estimated by CV, also exhibiting an opposite trend. Importantly, the values of IP_{PE} of **4** and **5** were found to be by *ca.* 0.15 eV lower than those of the earlier reported derivatives of TPA and naphthalimide in which the chromophores were linked via the linkages containing the single and double bonds.[25-27] Thus, the layers of compounds **4** and **5** are expected to exhibit lower injection barriers of holes from the electrode and therefore they could be more suitable for the electroluminescent devices.[56]

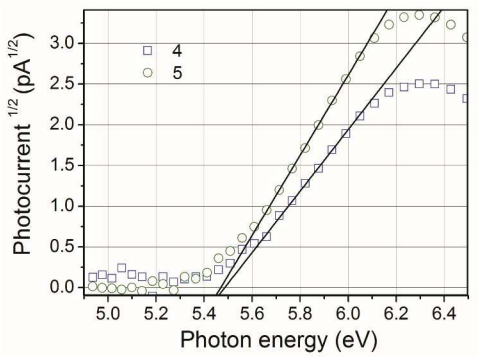

Figure 5. Electron photoemission spectra of the solid films of compounds **4** and **5**.

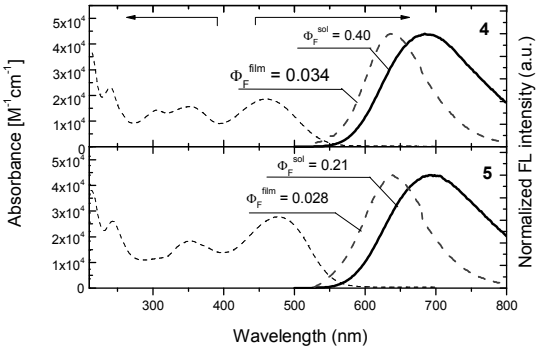

Figure 6. UV-vis (dashed thin line) spectra of 10^{-5} M solutions of **4, 5** in toluene; normalized fluorescence spectra of the dilute solutions in toluene (thick, solid line), and of the solid films (dashed grey line). The long-wavelength absorption maxima wavelengths were used as excitation wavelengths.

The theoretical IP^V values for **M4** and **M5** (6.09 and 5.98 eV, Table 2) exhibit a larger difference (-0.11 eV) as compared to IP_{CV} and IP_{PE} values (-0.03 and 0.02 eV, respectively). This might be due to the decreased dihedral angles and their variations in the solid state, making the influence of this factor on the HOMO energy being less important than in the gas phase (see section Geometry and electronic properties of model compounds).

Optical and photophysical properties

Absorption and fluorescence (FL) spectra of the dilute solutions (10^{-5} mol·L^{-1}) in non-polar toluene and of the solid films of the derivatives of TPA and naphthalimide (**4** and **5**) are shown in Figure 6. The wavelengths of the absorption maxima, molar extinction coefficients (ε), the wavelengths of fluorescence maxima, fluorescence quantum yields (Φ_F), Stokes shifts observed for the dilute solutions in seven different organic solvents are summarized in Table 3.

Table 3. Summary of absorption and emission properties of the solutions of **4** and **5** in various solvents and of the solid films of the compounds.

Solvent (viscosity ×10^{-3} Pas/ Dipole moment (D))	**4**			**5**		
	λ_{abs}/ nm[a] (ε/ M^{-1}cm^{-1})	λ_{em}/[b] nm (Φ_F)[c]	Stokes shift /nm, cm^{-1}	λ_{abs}/ nm[a] (ε/ M^{-1}cm^{-1})	λ_{em}/[b] nm (Φ_F)[c]	Stokes shift /nm, cm^{-1}
Cyclohexane (0.898/0)	457 (1.43)	523, 563 (0.51)	106, 4120	466 (2.57)	527, 567 (0.72)	101, 3823
Toluene (0.552/0.36)	460 (1.88)	594 (0.40)	134, 4904	443 (2.76)	583 (0.21)	107, 5421
THF (0.461/1.75)	461 (1.34)	686 (0.14)	225, 7115	476 (1.69)	696 (0.081)	220, 6641
Acetone (0.304/2.88)	463 (1.27)	753 (0.15)	295, 8318	464 (1.45)	752 (0.067)	288, 8254
Acetonitrile (0.3409/3.92)	465 (0.86)	758 (0.13)	294, 8313	468 (1.23)	755 (0.065)	284, 8122
Solid film	528	640 (0.034)	112, 3315	532	644 (0.028)	112, 3269

[a] λ_{abs} – absorption maximum; [b] λ_{em} – emission maximum; [c] Φ_F – Quantum yield.

The theoretical absorption spectra (Figure S3, see Supporting Information) indicate that the absorption bands in the range between 300 and 355 nm correspond to π-π* transitions mixing together local TPA and local naphthalimide, with different degree of ICT transitions. The low energy absorption bands between 457 and 491 nm correspond to HOMO→LUMO transitions. Given the dominant localization of these orbitals on the TPA and naphthalimide moieties, respectively, an intramolecular charge transfer (ICT) can be deduced for this band in both compounds (Figure 3 and Figure S3, Supporting Information). This band exhibits bathochromic and hyperchromic shifts with the increase of the number of naphthalimide moieties. The absorption maxima of the solid films of compounds **4** and **5** show red shifts of 68 and 56 nm, respectively with respect of those of dilute toluene solutions. This observation indicates that there are significant conformational changes of compounds **4** and **5** in the solid state with respect of those characteristic of the dilute solutions. Using the onset wavelengths of the absorption bands, the optical band gaps (E_g^{opt}) were estimated for compounds **4** and **5**. E_g^{opt} of compound **5** was evaluated at 2.22 eV, which is by 0.06 eV lower than that of the derivative **4** (2.28 eV). This observation can be explained the faster decrease of LUMO *versus* HOMO energy in compound **5** as compared to **4**. The values of E_g^{opt} observed for the solid films **4** and **5** were found to be by *ca.* 0.15 eV lower than those of the dilute solutions.

The emission maxima of the dilute toluene solutions of compounds **4**, **5** appear in the yellow-orange region at 594 nm and 583 nm (Figure 6). Broad and structureless FL spectra were obtained for the solid films of **4**, **5.** Their maxima peaking at 640 and 644 nm, respectively exhibit considerable red shifts with respect to the spectra of the dilute solutions. The Stokes shift for all solutions decrease with the increase of the number of naphthalimide arms (Table 3), but remain constant (112 nm) for the solid films of compounds **4** and **5**.

In a previous work we reported on derivatives of TPA and naphthalimide in which the chromophores were linked *via* the linkages containing single bonds[28] (Figure 7).

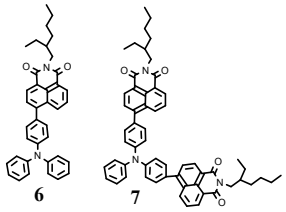

Figure 7. Structures of the previously reported compounds **6** and **7**.[28]

The dilute solutions of **4** and **5** in cyclohexane were found to exhibit red-shifted absorption by 44 and 56 nm as compared to those of compounds **6** and **7**. The fluorescence intensity maxima of the dilute solutions of compounds **4** and **5** also exhibited considerable red shifts (of 93 and 102 nm, respectively) relative to those of the solutions of **6** (470 nm) and **7** (465 nm).[28]

To investigate in detail the effect of solvatochromism of compounds **4** and **5**, the spectral changes induced by solvent polarity were estimated by comparison of the absorption and FL spectra of each compound using five solvents of different polarity with dielectric constants ranging from 2.02 to 37.50, including cyclohexane (dipole moment = 0 D), toluene (0.36 D), THF (1.75 D), acetone (2.91 D), and acetonitrile (3.92 D).

Figure 8 shows the effect of solvent polarity on FL spectra of the dilute solutions of compounds **4, 5**.

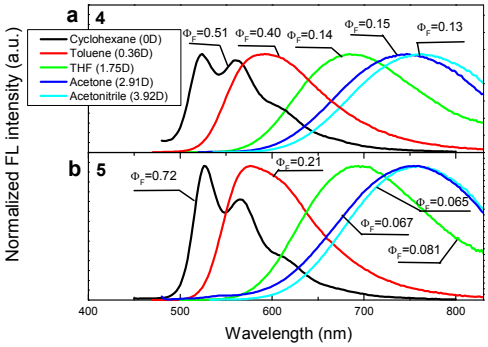

Figure 8. FL spectra of the dilute solutions (10^{-5} M) of compounds **4** (a) and **5** (b) in cyclohexane, toluene, THF, acetone and acetonitrile. The long-wavelength absorption maxima wavelengths were used as excitation wavelengths.

FL spectra of the dilute solutions of compounds **4**, **5** in cyclohexane show three peaks, which can be associated with the transitions from the lowest vibrational excited state to three different vibrational ground states (0→0, 0→1, and 0→2).[57,58] As the solvent polarity increased, the FL spectra of the studied compounds become structureless and exhibit only a single broad band. The solutions of compounds **4, 5** in polar solvents show red shifted FL intensity maxima compared to those observed for the solutions in nonpolar solvents. This suggests ICT occurring from the less polar ground state to the more polar excited state.[59] Indeed, triplet state calculations of model compounds **M4** and **M5** in the geometry of the ground state result in large dipole moments of 14.4 and 12 D, respectively, as compared to 8.1 and 7.1 D, respectively for the singlet ground state. This is also suported by the increasing Stokes shifts with the increasing solvent polarity, in turn indicating that the polar excited state is more stabilized in the polar solvents.

The spectral dependency on the solvent polarity was studied on the basis of the Lippert-Mataga model. The Lippert-Mataga polarity parameter (Δ*f*, also called orientation polarizability parameter) was considered as a measure of the polarity of the different solvents used. It was calculated according to the following equation 2:[60]

$$\nu_A - \nu_F = 2/hc \times \Delta\mu^2 \times \Delta f \times a^{-3} + const.$$
$$\Delta f = (\varepsilon - 1)/(2\varepsilon + 1) - (n^2 - 1)/(2n^2 + 1), \qquad \Delta\mu = \mu_E - \mu_G$$
$$(\nu_A - \nu_F)/\Delta f = 11307.6\Delta\mu^2 \times a^{-3} + const. \qquad (2)$$

where ν_A and ν_F are the wavenumbers (cm^{-1}) of the absorption and emission maxima, respectively, h = 6.6256×10^{-27} erg s (Planck's constant); c = 2.9979×10^{10} cm s^{-1} (the speed of light); a is the radius of the cavity in which the fluorophore resides; μ_G and μ_E refer to the ground state and excited state dipole moments, respectively. The slope of the Lippert plot reflects the solvent sensitivity of a fluorophore.

The Lippert-Mataga plot has to be linear, provided the solvent-solute interactions are dipolar. Figure 9a suggests linear correlations between the Stokes shift of compounds **4, 5** and the solvent orientation polarizability.

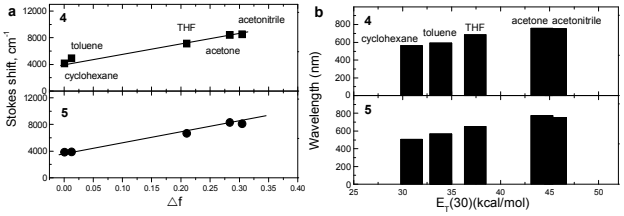

Figure 9. (a) Dependences of Stokes shifts Δν of compounds **4, 5** (c = 10^{-5} M) on the orientation polarizability *Δf*. The solid lines correspond to the linear fits. (b) Plots of the wavelengths of fluorescence intensity maxima of **4, 5** *versus* $E_T(30)$ polarity parameter of the different solvents.

For the description of solvatochromism of compounds **4** and **5**, the Reichardt-Dimroth equation was additionally used 3:[61]

$$\nu_A - \nu_F = m_4 \cdot E_T^N + const. \qquad (3)$$

E_T^N, the normalized solvent polarity of Reichardt is a solvatochromic parameter based on the absorption wavenumber of a standard betaine dye in the corresponding solvent. A linear correlation between the position of the emission maxima and empirical solvent polarity parameter ($E_T(30)$) was observed for the solutions of compounds **4, 5** in aprotic solvents (Figure 9b), again revealing the involvement of solvent polarity dependent ICT emissive states.

The values of Φ_F of the solutions of the synthesized compounds in different solvents were also estimated. They are summarized in Table 3. Viscosity of the solvents as well as the polarity seems to have influence on Φ_F of the compounds. The highest Φ_F values (0.51 and 0.72 for **4** and **5**, respectively, Table 3) were found in the case of cyclohexane solutions with the highest viscosity and the lowest dielectric constant (2.02) of the solvent (0.898×10^{-3} Pas). Higher fluorescence quantum

efficiencies were observed for the solutions in non-polar solvents compared to those in polar solvents, with the lower viscosity values and with the lowest emission intensity found in acetonitrile (Table 3). This is probably due to the enhanced ICT from the TPA to the naphthalimide moieties through the olefinic spacers. Indeed, ICT is considered to reduce the quantum yield due to more pronounced relaxation and nonradiative decay of the excited states.[62] The globally smaller Φ_F values for compound **5** as compared to **4** (except for the cyclohexane solution) seem to comfort the above assumption, as the red shifted ICT for **5** are expected to enhance the nonradiative decay as compared to **4**. However, enhancement of exciplex formation with increasing solvent polarity may additionally contribute to the decreased quantum yields, which is supported by the smallest Φ_F values found for both compounds in the less polar solid state (0.034 and 0.028 for **4** and **5,** respectively, Table 3).

Hole transport properties

The charge transporting properties of the compounds were probed by the xerographic time-of-flight (XTOF) method. For the layers of compounds **4** and **5** hole mobilities were found to be 2.1×10^{-3} and 2.2×10^{-4} cm^2/Vs at the electric fields of 2.4×10^5 and 6.1×10^5 V/cm, respectively. The layers of the molecular mixtures of compounds **4** and **5** with PC-Z (50%) were also prepared. Charge transporting characteristics of compounds **4** and **5** are summarized in Table 4.

XTOF transients exhibited dispersive charge transport for all the samples and the transient-time (t_t) values were determined from the kinks of photocurrent curves in double logarithmic plots (Figure 10a). As such, these hole mobilities are expected to characterise the fastest carriers instead of the steady state hole transport of these materials. However, the dependence of the square root of the applied electric field (E) on the logarithm of hole mobility (μ_h) was found to be linear for all the samples investigated (Figure 10b). Such electric field dependence on hole mobility follows the nearly universal Poole-Frenkel relationship ($\mu = \mu_0 \exp(\alpha E^{1/2})$). This relationship is usually observed in disordered organic systems[63] and can be attributed to effects of energetic and positional disorder on the hopping conduction in amorphous organic solids. Carrier transport in an amorphous organic solid that can be commonly described by Marcus theory[64] is generally associated with charge carriers hopping along channels of localized hopping sites. Due to disorder phenomena, the distribution of the hoping site energies (width of the density of states, DOS) is generally large, so that the charge transport in amorphous materials is generally disorder dominated. In order to estimate the role of the polaronic-type transport, we compare the intrinsic properties of compounds **4** and **5**. In the frame of Marcus theory, the charge hopping rates between identical molecules basically depend on the intramolecular reorganization energy (λ_i), and the electronic couplings between the HOMOs of adjacent molecules (limited to a monoelectronic approximation). In order to evaluate the electronic couplings, a selected number of dimers were constructed from the model compounds **M4** and **M5** (Figure 11 and Figure S4, Supporting Information). Our calculations indicate: (i) decreasing intramolecular reorganization energy from 0.23 to 0.14 eV for compounds **4** and **5,** respectively, which predicts evolution of hole mobility in opposite sens as compared to the esperimental results. (ii) Non-negligible HOMO-HOMO electronic couplings of roughly 0.01-0.08 eV were calculated (Table 5), suggesting good intrinsic properties for hole transport. However, increased average intermolecular distances and decreased HOMO-HOMO electronic couplings were found for compound **5** as compared to **4**, suggesting a slight advantage for the hole transport in layers of compound **4**.

All in all, the evolutions of intramolecular reorganization energy parameter and electronic couplings should roughly cancel out, thus suggesting negligible influence of polaronic type mechanism on the hole transport in these materials. Note that the enhanced space extension of HOMO distribution in **M5** as compared to **M4** (Figure 3) would suggests enhanced possibilities for efficient electronic couplings between HOMOs on relatively distant adjacent molecules, but this would be in opposite agreement with the experimental trend of hole mobilities. Both parameter trends thus result in polaronic-type transport predictions which are unable to account for the larger hole mobility by one order of magnitude in **4** as compared to **5**. The increased hole mobility observed in compound **4** is then likely to be due to the smaller degree of disorder in the layers of this compounds as compared to **5**, which could stem form two effects: (i) due to a larger dipole moment of **M4** as compared to **M5** (8.1 and 7.1 D, respectively) and probably due to a smaller steric repulsion, stronger intermolecular interactions can be supposed for compound **M4**, assumably resulting in denser molecular packing in the layers of this compound. Indeed, the calculated average intermolecular distances for some selected dimers are systematically smaller for **M4** than for **M5** (Table 5). Interestingly, the increasing intermolecular interaction energies and the reduced intermolecular distances were recently shown to result in reduced geometrical randomness and decreased distribution of HOMO energies.[29] (ii) The number of dihedral angles between groups contributing to HOMO is larger in compound **5** (Figure 3). This suggests enhanced impact of geometrical deformations on the HOMO energy, which are expected to negatively impact the hole mobility by means of increasing width of DOS. Both factors predict larger value of the σ parameter (standard deviation of the DOS distribution) for **5** as compared to **4**, which seems consistent with the larger α value of **5** (Table 4). Nevertheless, the hole mobilities observed for **4** and **5** were found to be comparable to those of the other compounds consisting of TPA core and naphthalimide arms.[27-29]

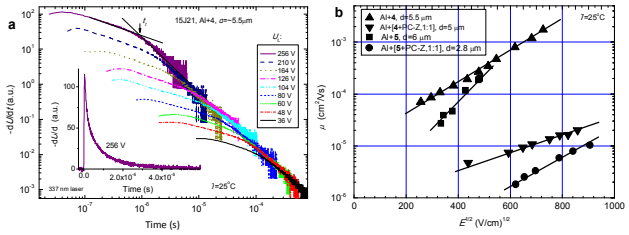

Figure 10. Transient photocurrents for the layer of compound **4** at different applied sample voltages (a); electric field dependencies of hole drift mobilities for the layers of **4** and **5** (b).

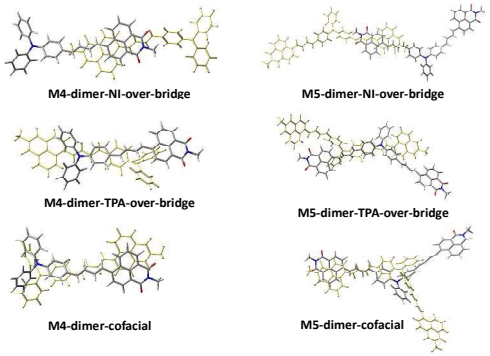

Figure 11. Selected choice of dimers constructed from the model compounds **M4** and **M5**, obtained at the ωB97XD/6-31G(d,p) level in gas phase. The dimer indicated as „naphthalimide-over-bridge", for instance, corresponds to naphthalimide moiety over the butadiene one. See Figure S4 (Supporting Information) for additional dimer types for the model compound **M4**.

Table 4. Charge transporting properties of the layers of **4** and **5** and of their solid solutions with PC-Z.

Neat layers		
Compound	**4**	**5**
Layer thickness (μm)	5.5	6.0
μ_h (cm^2/Vs)[a]	2.1×10^{-3}	2.2×10^{-4}
α ($cm^{1/2}/V^{1/2}$)[b]	0.0068	-
Layer with PC-Z (weight ratio 1:1)		
Compound	**4**	**5**
Layer thickness (μm)	5.0	2.8
μ_h (cm^2/Vs)[a]	2.1×10^{-5}	1.1×10^{-5}
α ($cm^{1/2}/V^{1/2}$)[b]	0.0034	0.0061

[a] μ_h – hole drift mobility value; [b] α – Pool-Frenkel parameter for holes.

Table 5. HOMO-HOMO electronic couplings and average intermolecular distance for a selected choice of dimers constructed from the model compounds **M4** and **M5**. The dimers are indicated as „naphthalimide-over-bridge" (corresponding to naphthalimide moiety over the butadiene one), „cofacial", and „TPA-over-bridge" (Figure 11 and Figure S4 (Supporting Information)). The electronic couplings are calculated at the B3LYP/6-31G(d,p)/ ωB97XD/6-31G(d,p) level in gas phase. The average distances correspond to the molecular moieties of adjacent moleculas in direct contact.

		Dimer-naphthalimide-over- naphthalimide	Dimer-naphthalimide-over-bridge	Dimer-cofacial	Dimer-TPA-over-bridge	Dimer-TPA-over-TPA	Dimer-naphthalimide-over-TPA
t (eV)	**4**	0.006	0.035	0.083	0.043	0.028	0.007
	5	-	0.024	0.072	0.008	-	-
	Δ(**5-4**)	-	-0.011	-0.011	-0.035	-	-
d (Å)	**4**	3.496	3.611	3.650	3.843	3.804	3.694
	5	-	3.668	3.727	3.938	-	-
	Δ(**5-4**)	-	0.057	0.078	0.095	-	-

Conclusions

Solution-processable derivatives of triphenylamine and 1,8-naphthalimide with the olefinic linkages between chromophores were synthesized by Heck reaction. Their thermal, optical, electrochemical and photoelectrical properties were studied and discussed in terms of the correlation with the chemical structures and compared with those of the earlier reported derivatives of triphenylamine and 1,8-naphthalimide with the single bonds between chromophores. The compounds showed high thermal stability with the 5% weight loss temperatures of 350 and 363 °C. They form glasses with glass transition temperatures of 56 and 75 °C. The solution of the compound with two 1,8-naphthalimide moieties in cyclohexane exhibits the emission quantum yield of 0.72. Due to pronounced electron donor-acceptor character, the compounds showed solvatochromic red shifts of fluorescence up to 158 nm with significant reduction of the emission yield. The ionization potential values of the synthesized compounds measured by the cyclic voltammetry are 5.22 and 5.27 eV and electron affinities – -3.20 and -3.18 eV. The ionization potentials estimated by electron photoemission technique were found to be 5.47 and 5.49 eV. Xerographic time-of-flight hole mobility of the layer of *N*-(4-((E)-buta-1,3-dienyl)phenyl)-*N*-phenyl-(*N*-(2-ethylhexyl)-1,8-naphthalimide) exceeds 2.1×10^{-3} cm^2/Vs at the electric field of 2.4×10^5 V/cm. The trend in intrinsic hole transport parameters predicted by theoretical estimations in the frame of Marcus theory is opposite to the experimental one, suggesting for these materials disorder dominated hole transport.

Acknowledgements

This article was prepared under the support of the European Social Fund Agency implementing measure VP1-3.1-ŠMM-08-K of the Human Resources Development Operational

Programme of Lithuania 2007–2013 third priority "Strengthening of capacities of researchers and scientists" (project No. VP1-3.1-ŠMM-08-K-01-013). Dr. D. Volyniuk is thanked for the help in ionization potential measurements.

Notes and references

1 C. Q. Ma, M. Fonrodona, M. C. Schikora, M. M. Wienk, R. A. J. Janssen and P. Bauerle, *Adv. Funct. Mater.,* 2008, **18**, 3323.
2 A. Pron, P. Gawrys, M. Zagorska, D. Djurado and R. Demadrille, *Chem. Soc. Rev.,* 2010, **39**, 2577.
3 S. Chen, X. Xu, Y. Liu, G. Yu, X. Sun, W. Qiu, Y. Ma and D. Zhu, *Adv. Funct. Mater.,* 2005, **15**, 1541.
4 Z. Li, Z. Wu, W. Fu, P. Liu, B. Jiao, D. Wang, G. Zhou and X. Hou, *J. Phys. Chem. C,* 2012, **116***,* 20504.
5 N. Metri, X. Sallenave, C. Plesse, L. Beouch, P. H. Aubert, F. Goubard, C. Chevrot and G. Sini, *J. Phys. Chem. C,* 2012, **116***,* 3765.
6 S. A. Bagnich, S. Athanasopoulos, A. Rudnick, P. Schroegel, I. Bauer, N. C. Greenham, P. Strohriegl and A. Köhler, *J. Phys. Chem. C,* 2015, **119**, 2380.
7 H. Choi, S. Paek, N. Lim, Y. H. Lee, M. K. Nazeeruddin and J. Ko, *Chem. Eur. J.,* 2014, **20**, 10894.
8 J. Li, D. Liu, Z. R. Hong, S. W. Tong, P. F. Wang, C. W. Ma, O. Lengyel, C. S. Lee, H. L. Kwong and S. Lee, *Chem. Mater.* 2003, **15**, 1486.
9 C. Lambert, J. Schelter, T. Fiebig, D. Mank and A Trifonov, *J. Am. Chem. Soc.,* 2005, **127**, 10600.
10 S. Roquet, A. Cravino, P. Leriche, O. Aleveque, P. Frere and J. Roncali, *J. Am. Chem. Soc.,* 2006**, 128**, 3459.
11 A. Leliege, J. Grolleau, M. Allain, P. Blanchard, D. Demeter, T. Rousseau and J. Roncali, *Chem. Eur. J.,* 2013, **19,** 9948.
12 Z. J. Ning and H. Tian, *Chem. Commun.,* 2009, **37***,* 5483.
13 M. Greatzel, *Acc. Chem. Res.,* 2009, **42***,* 1788.
14 Z. Jiang, T. Ye, C. Yang, D. Yang, M. Zhu, C. Zhong, J. Qin and D. Ma, *Chem. Mater.,* 2011, **23**, 771.
15 T. Lee, C. L. Landis, B. M. Dhar, B. J. Jung, J. Sun, A. Sarjeant, J. J. Lee and H. E. Katz, *J. Am. Chem. Soc.,* 2009, **131***,* 1692.
16 R. Zalesny, O. Loboda, K. Iliopoulos, G. Chatzikyriakos, S. Couris, G. Rotas, N. Tagmatarchis, A. Avramopoulos and M. G. Papadopoulos, *Phys. Chem. Chem. Phys.,* 2010, **12***,* 373.
17 K. Ghosh, G. Masanta, R. Fröhlich, I. D. Petsalakis and G. Theodorakopoulos, *J. Phys. Chem. B,* 2009, **113***,* 7800.
18 T. T. Bui, L. Beouch, X. Sallenave and F. Goubard, *Tetrahedron Lett.,* 2013, **54***,* 4277.
19 H. Zhou, Z. Zheng, G. Xu, Z. Yu, X. Yang, L. Cheng, X. Tian, L. Kong, J. Wu and Y. Tian, *Dyes Pigm.,* 2012, **94***,* 570.
20 M. G. Vivas, D. L. Silva, J. Malinge, M. Boujtita, R. Zalesny, W. Bartkowiak, H. Agren, S. Canuto, L. De Boni, E. Ishow and C. R. Mendonca, *Sci. Rep.,* 2014, **4***,* 1.
21 J. Liang, C. Zhu and Z. Cao, *Phys.Chem. Chem. Phys.,* 2013, **15***,* 13844.
22 M. Planells, A. Abate, D. J. Hollman, S. D. Stranks, V. Bharti, J. Gaur, D. Mohanty, S. Chand, H. J. Snaith and N. Robertson, *J. Mater. Chem. A,* 2013, **1***,* 6949.
23 E. B. Veale and T. Gunnlaugsson, *J. Org. Chem.,* 2008, **73***,* 8073.
24 D. Gudeika, J. V. Grazulevicius, D. Volyniuk, R. Butkute, G. Juska, A. Miasojedovas, A. Gruodis and S. Jursenas, *Dyes Pigm.*, 2015, **114**, 239.
25 D. Gudeika, R. R. Reghu, J. V. Grazulevicius, G. Buika, J. Simokaitiene, A. Miasojedovas, S. Jursenas and V. Jankauskas, *Dyes Pigm.*, 2013, **9**, 895.
26 A. Furstenberg and E. Vauthey, *Photochem. Photobiol. Sci.,* 2005, **4***,* 260.
27 D. Gudeika, A. Michaleviciute, J. V. Grazulevicius, R. Lygaitis, S. Grigalevicius, V. Jankauskas, A. Miasojedovas, S. Jursenas and G. Sini, *J. Phys. Chem. C,* 2012, **116**, 14811.
28 D. Gudeika, J. V. Grazulevicius, G. Sini, A. Bucinskas, V. Jankauskas, A. Miasojedovas and S. Jursenas, *Dyes Pigm.,* 2014, **106**, 58.
29 D. Gudeika, J. V. Grazulevicius, D. Volyniuk, G. Juska, V. Jankauskas and Gjergji Sini, *J. Phys. Chem. C,* 2015, DOI: 10.1021/acs.jpcc.5b10163.
30 J. C. Mello, H. F. Wittmann and R. H. Friend, *Adv. Mater.,* 1997, **9**, 230.
31 G. Gritzner and J. Kuta, *Pure Appl. Chem.,* 1984, **56**, 461.
32 E. Miyamoto, Y. Yamaguchi and M. Yokoyama, *Electrophotography,* 1989, **28**, 364.
33 E. Montrimas, V. Gaidelis and A. Pazera, *Lithuanian J. Phys.,* 1996, **6**, 569.
34 L. M. Harwood and C. J. Moody, Blackwell Science, 1989.
35 D. Gudeika, R. Lygaitis, V. Mimaite, J. V. Grazulevicius, V. Jankauskas, M. Lapkowski and P. Data, *Dyes Pigm.,* 2011, **91**, 13.
36 X. Yang, Y. Zhao, X. Zhang, R. Li, J. Dang, Y. Li, G. Zhou, Z. Wu, D. Ma, W. Y. Wong, X. Zhao, A. Ren, L. Wang and X. Hou, *J. Mater. Chem.,* 2012, **22**, 7136.
37 M. L. Keshtov, M. I. Buzin, P. V. Petrovskii, E. E. Makhaeva, V. S. Kochurov, D. V. Marochkin and A. R. Khokhlov, *Polym. Sci. Ser. B,* 2011*,* **53***,* 257.
38 F. Terenziani, C. Le Droumaguet, O. Mongin, C. Katan and M. Blanchard-Desce, *Nonlinear Optics, Quantum Optics-Concepts in Modern Optics,* 2006*,* **35***,* 69.
39 M. Mitsuyuki, M. Tetsuro and S. Atsuro, *Jpn. Kokai Tokkyo Koho* 1997, JP 09297415 A, 19971118.
40 J. Pei, M. Liang, J. Chen, Z. L. Tao and W. Xu, *Acta Phys-Chim. Sin.,* 2008*,* **24***,* 1950.
41 W. Kohn and L. Sham, *J. Phys. Rev.,* 1965, **140**, A1133.
42 C. T. Lee, W. T. Yang and R. G. Parr, *Phys. Rev. B,* 1988, **37**, 785.
43 A. D. Becke, *J. Chem. Phys.,* 1993, **98**, 5648.
44 J. D. Chai and M. Head-Gordon, *Phys. Chem. Chem. Phys.,* 2008, **10**, 6615.
45 M. J. Frisch, G. W. Trucks, H. B. Schlegel, G. E. Scuseria, M. A. Robb, J. R. Cheeseman, G. Scalmani, V. Barone, B. Mennucci, G. A. Petersson, H. Nakatsuji, M. Caricato, X. Li, H. P. Hratchian, A. F. Izmaylov, J. Bloino, G. Zheng, J. L. Sonnenberg, M. Hada, M. Ehara, K. Toyota, R. Fukuda, J. Hasegawa, M. Ishida, T. Nakajima, Y. Honda, O. Kitao, H. Nakai, T. Vreven, J., J. A. Montgomery, J. E. Peralta, F. Ogliaro, M. Bearpark, J. J. Heyd, E. Brothers, K. N. Kudin, V. N. Staroverov, T. Keith, R. Kobayashi, J. Normand, K. Raghavachari, A. Rendell, J. C. Burant, S. S. Lyengar, J. Tomasi, M. Cossi, N. Rega, J. M. Millam, M. Klene, J. E. Knox, J. B. Cross, V. Bakken, C. Adamo, J. Jaramillo, R. Gomperts, R. E. Stratmann, O. Yazyev, A. J. Austin, R. Cammi, C. Pomelli, J. W. Ochterski, R. L. Martin, K. Morokuma, V. G. Zakrzewski, G. A. Voth, P. Salvador, J. J. Dannenberg, S. Dapprich, A. D. Daniels, O. Farkas, J. B. Foresman, J. V. Ortiz, J. Cioslowski and D. J. Fox, 2009, Gaussian 09, Revision B.01, Gaussian Inc., Wallingford CT, 2010.
46 E. K. U. Gross and W. Kohn, *Phys. Rev. Lett.,* 1985, **55**, 2850.
47 E. Runge and E. K. U. Gross, *Phys. Rev. Lett.,* 1984, **52**, 997.
48 E. K. U. Gross and W. Kohn, *Adv. Quant. Chem.,* 1990, **21**, 255.
49 R. Bauernschmitt and R. Ahlrichs, *Chem. Phys. Lett.,* 1996, **256**, 454.
50 M. E. Casida, C. Jamorski, K. C. Casida and D. R. Salahub, *J. Chem. Phys.*, 1998, **108**, 4439.
51 R. Dennington II, T. Keith and J. Millam, GaussView, Version 5, Semichem Inc., Shawnee Mission KS, 2009.

52 J. L. Bredas, D. Beljonne, V. Coropceanu and J. Cornil, *Chem. Rev.,* 2004, **104**, 4971.
53 M. D. Newton, *Chem. Rev.,* 1991, **91**, 767.
54 E. F. Valeev, V. Coropceanu, D. A.da Silva, S. Salman and J. L. Bredas, *J. Am. Chem. Soc.,* 2006, **128**, 9882.
55 K. Senthilkumar, F. C. Grozema, F. M. Bickelhaupt and L. D. A. Siebbeles, *J. Chem. Phys.,* 2003, **119**, 9809.
56 H. Xu, R. Meng, C. Xu, J. Zhang, G. He and Y. Cui, *Appl. Phys Lett.,* 2003, **83**, 1020.
57 J. Franck, *J. Chem. Soc. Faraday Trans.,* 1926, **21**, 536.
58 E. Condon, *Phys. Rev.,* 1926, **27**, 640.
59 E. Ishow, G. Clavier, F. Miomandre, M. Rebarz, G. Buntinx and O. Poizat, *Phys. Chem. Chem. Phys.,* 2013, **15**, 13922.
60 P. R. Bangal, S. Panja and S. Chakravorti, *J. Photochem. Photobiol. A,* 2001, **139**, 5.
61 C. Reichardt and T. Welton, Solvents and solvents effects in organic chemistry, 4th ed., Wiley-VCH, Weinheim, 2011.
62 J. Sung, P. Kim, Y. O. Lee, J. S. Kim and D. Kim, *J. Phys. Chem. Lett.,* 2011, **2**, 818.
63 H. Bassler, *Int. J. Mod. Phys. B* 1994, **8**, 847.
64 R. A. Marcus, *Rev. Mod. Phys.,* 1993, **65**, 599.

Graphical Abstract